

A facile synthesis of layered double hydroxide based core@shell hybrid materials

Meng Lyu, Chunping Chen, Jean-Charles Buffet, and Dermot O'Hare *

Received 00th January 20xx,
Accepted 00th January 20xx

DOI: 10.1039/x0xx00000x

Zeolite@LDH core-shell hybrid (13X@Mg₂Al-CO₃) and MOF@LDH core-shell hybrid Mg-MOF-74@Mg₂Al-CO₃ have been synthesised using a simple, scalable co-precipitation method. The effects of the synthesis parameters on the phase purity, crystallinity, morphology, composition, thermal stability and BET specific surface area of the core-shell hybrid have been investigated.

Introduction

Layered double hydroxides (LDHs) are a family of naturally occurring layered (2D) minerals, they are built of alternative stacking of positively charged metal hydroxide layers and negatively charged molecular-based anionic layers.^{1,2} A generalised formula of an LDH can be represented by $[(M_{1-x}^{z+}M_x^{y+}(OH)_2)]^{w+}(A^{n-})_{w/n} \cdot mH_2O$, where M and M' are monovalent/divalent and trivalent/ tetravalent metal cations respectively, and Aⁿ⁻ represents the interlayer anions, ($w = z(1-x) + xy - 2$; since w must be positive real, when $z = 1$ and $y = 3$ then $x \geq 0.5$; more commonly $z = 2$ and $y = 3$ thus $x > 0$ but practically x is found to give phase pure LDHs when in the range $0.35 \leq x \leq 0.16$). LDHs have found practical applications in catalysts,³ supercapacitors,⁴ gas separation,⁵ and drug delivery.⁶ Recently, research has been directed at the synthesis of core-shell materials with LDH as the shell and silica,^{7–11} zeolite,¹² carbon,^{13,14} and metal oxides^{15,16} as the core.

The core@shell structure allows to combine the physiochemical features from both LDHs and the core materials, which allows the design of nanocomposites with features such as high surface area, magnetism and synergistic catalysis.¹⁷ For example, we have shown that core@LDH hybrids exhibit synergistic behaviour; Buffet *et al.* reported using silica@LDH and zeolite@LDH as catalyst support for slurry-phase ethylene polymerisation. These core-shell systems shows up to three times higher catalytic productivity compared to the core or shell system alone.¹⁸ Wang *et al.* reported Cu₂O@ZnCr-LDH core-shell photocatalyst that exploited the band gap matching between Cu₂O and ZnCr-LDH to achieve an enhanced catalytic activity and photostability towards the water splitting

reaction.¹⁹ Li *et al.* reported Co₃O₄@NiCoAl-LDH core-shell nanowire and attributed the improved electrochemical performance and cycling stability to a synergistic effect.²⁰ Ni *et al.* reported that a porous graphitised carbon@NiFe-LDH had an outstanding catalytic activity and admirable stability towards oxygen evolution (OER) reaction was attributed to an increased exposure of active sites compared with the pure NiFe LDH.²¹ Othman *et al.* showed that an Mg_xAl-LDH coated zeolite exhibits higher CO₂ capture capacity and selectivity compared to pure the pristine zeolite.²²

Zeolites, a family of porous crystalline aluminosilicates, are well-known for their low cost and high chemical stability. Zeolite 13X, also known as molecular sieve NaX, is a porous Na-exchanged faujasite-type (FAU) zeolite with chemical formula $[Na_{88}(AlO_2)_{88}(SiO_2)_{104} \cdot nH_2O]$.^{23,24} Zeolite 13X has been commercially exploited as catalyst^{25,26} and gas adsorbent.^{27,28}

M-MOF-74 are crystalline metal-organic-framework (MOF) materials (M = Mg, Ni or Co). The MO₅ polyhedra coordinate with the deprotonated 2,5-dihydroxy-1,4-benzene-dicarboxylic acids to afford the framework structure of M-MOF-74. By substitution of the metal cations in the framework, the properties of M-MOF-74 can be modified. M-MOF-74's are widely used in gas separation,^{29,30} catalysis,³¹ supercapacitors³² and for drug delivery.³³

It is expected that core-shell composites, using zeolite (or M-MOF-74) core and LDH shell, could exhibit the distinguish property of both zeolite (or M-MOF-74) and LDH and perform outstanding catalytic ability or gas adsorption property.

Herein, we explore the synthesis of zeolite 13X@Mg₂Al-CO₃ LDH. Effect of reagent addition rate and reaction ageing time, on the LDH shell growth, morphology and surface area of core-shell has been systematically studied. The optimised synthetic conditions were then successfully applied on another core material, Mg-MOF-74.

Chemistry Research Laboratory, Department of Chemistry, University of Oxford, 12 Mansfield Road, Oxford, OX1 3TA, UK. E-mail: dermot.ohare@chem.ox.ac.uk; Tel: +44(0)1865 272686

Electronic Supplementary Information (ESI) available: XRD, TEM, FTIR, TGA, BET, solid state NMR, ICP-MS and elemental analysis. See DOI: 10.1039/x0xx00000x

O which is equivalent to a 1:1 Z13X:Mg₂Al-CO₃ LDH stoichiometry.

Result and discussion

Synthesis and characterisation of Z13X@Mg₂Al-CO₃ LDH

Core-shell Z13X@Mg₂Al-CO₃ LDH was prepared using the co-precipitation method in which *in-situ* grow of the LDH platelets occurs on the surface of Z13X crystallites. A 2:1 molar solution of Mg and Al nitrates were added to an aqueous dispersion of Z13X in Na₂CO_{3(aq)} at pH 10. The pH of the reaction mixture was held at 10 using 1 M NaOH_(aq). The resulting reaction mixture was allowed to age for 1 hr after completion of the addition of the nitrate solutions. The solid product was collected by filtration and washed with water before drying under vacuum at 30 °C overnight. The product was a white powder (Z13X@Mg₂Al-CO₃ LDH). Chemical analysis is consistent with the composition

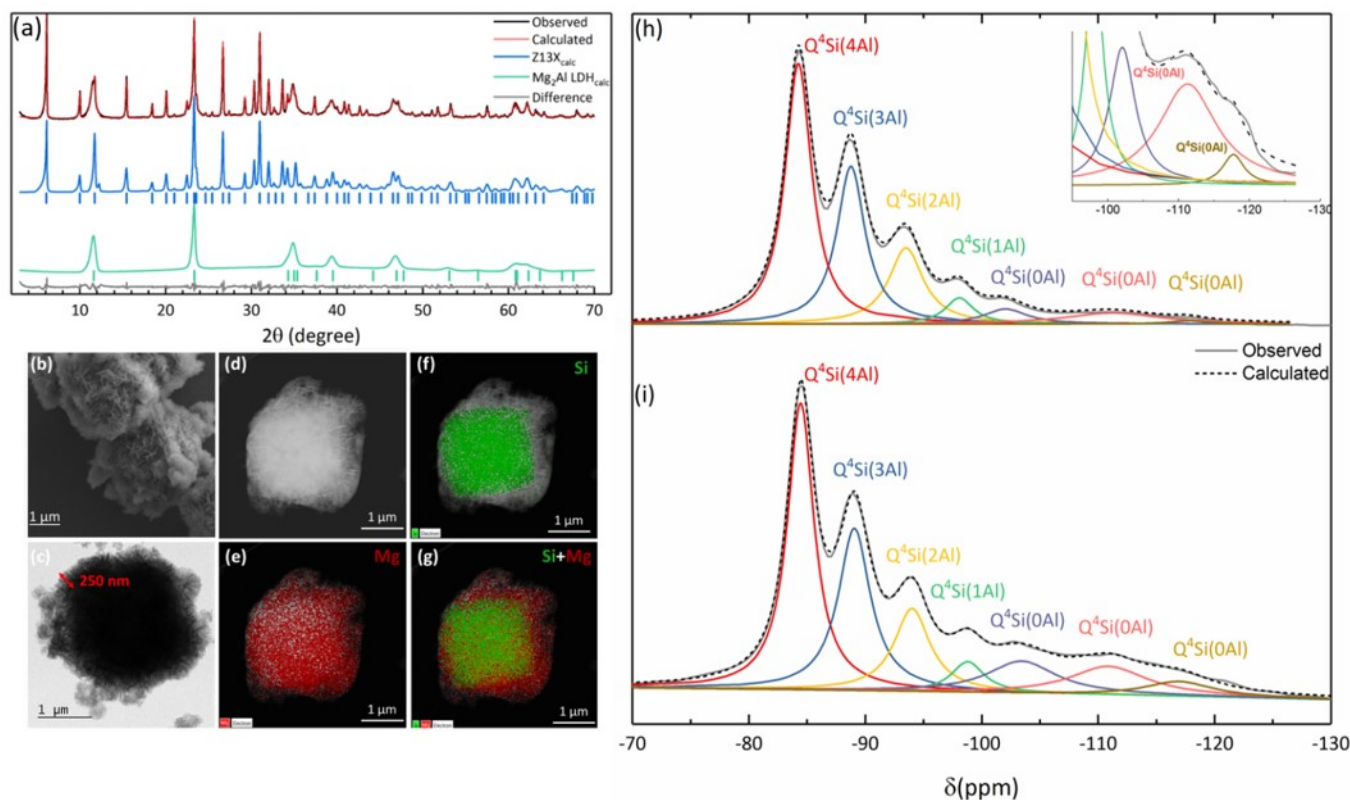
$$[H_{0.1}Na_{0.26}(AlO_2)_{0.36}(SiO_2)_{0.60}][Mg_{0.64}Al_{0.35}(OH)_{1.98}](CO_3)_{0.18} \cdot 1.5H_2O$$


Fig. 1. (a) XRD pattern and two-phase Pawley refinement of Z13X@Mg₂Al-CO₃ LDH. The observed, calculated and difference plots are shown in red and black respectively. The calculated XRD patterns for pure Z13X and Mg₂Al-CO₃ LDH are shown in blue and green respectively, (b) SEM image, (c) TEM image, (d) STEM image and (e)-(g) EDX elemental mapping images of Z13X@Mg₂Al-CO₃ LDH. ²⁹Si solid-state MAS NMR spectra of (h) Z13X and (i) Z13X@Mg₂Al-CO₃ LDH. The observed and calculated plots are shown using grey solid line and black dash line respectively. The insert graph is the zoom-in of Z13X.

The commercial zeolite 13X (Z13X) used in this work is a highly crystalline material exhibiting a uniform octahedra particle morphology (2–4 μm) with smooth edges (Fig. S1 and S2). In the the powder X-ray diffraction (XRD) of Z13X@Mg₂Al-CO₃ LDH we observe both Bragg diffraction

features of Z13X and Mg₂Al-CO₃ LDH, the separate contributions can be confirmed by the two-phase Pawley refinement³⁵ (Fig. 1a). The details of the two-phase Pawley refinement can be found in ESI (Fig. S3, Table S1). The transmission electron microscopy (TEM) and scanning

electron microscopy (SEM) of Z13X@Mg₂Al-CO₃ LDH shows that LDH nanosheets grow uniformly in a radial direction from the surface of Z13X crystallites to form a shell with a thickness *ca.* 250 nm (Fig. 1b-c). Energy dispersive X-ray spectroscopy (EDX) mapping showed that silicon atoms (green) from Z13X are mainly distributed at the inner core; with magnesium (red) from the Mg₂Al-CO₃ LDH homogeneously dispersed over the whole particle (Fig. 1d-g). The FTIR spectra of Z13X, Z13X@Mg₂Al-CO₃ LDH and Mg₂Al-CO₃ LDH are shown in Fig. S4. Z13X@Mg₂Al-CO₃ LDH exhibits characteristic IR absorbances from both the core and shell; the CO₃²⁻ stretching absorbance at 1360 cm⁻¹ and O-H bending mode at 3500 cm⁻¹ are from the LDH shell,¹ while ν(Si-O) stretching at 960 cm⁻¹ and ν(Al-O) vibration at 720 cm⁻¹ arise from the Z13X core.³⁶

The ²⁹Si and ²⁷Al solid-state nuclear magnetic resonance (ssNMR) spectra of Z13X and Z13X@Mg₂Al-CO₃ LDH are shown in Fig. 1 and S5. Fig. 1h shows that the Z13X core contains seven characteristic ²⁹Si NMR resonances. Five of them, from the framework of zeolite, are at -84.2, -88.8, -93.5, -98.1 and -102.0 ppm which can be assigned to Q⁴Si(4Al), Q⁴Si(3Al), Q⁴Si(2Al), Q⁴Si(1Al) and Q⁴Si(0Al) respectively (Table S2).³⁷ Two resonances at -111.2 and -117.7 ppm, assigned as Q⁴Si(0Al), may arise from either amorphous silicates or a pure Si zeolite domain inclusion within the Z13X sample.^{38,39} Core-shell Z13X@Mg₂Al-CO₃ LDH exhibits seven ²⁹Si NMR resonance (Fig. 1i, Table S2). Five of them are the corresponding resonance of Q⁴Si(4Al), Q⁴Si(3Al), Q⁴Si(2Al), Q⁴Si(1Al) and Q⁴Si(0Al) of the parent zeolite. After co-precipitation, these five resonances show a slight shift to lower field. Resonances corresponding to Si with Al nearest neighbours, Q⁴Si(4Al), Q⁴Si(3Al), Q⁴Si(2Al), Q⁴Si(1Al), exhibit a lower intensity. The resonance assigned to non-Al neighbours, Q⁴Si(0Al), increases in relative intensity. We believe this is due to loss of Al and/or Na from the zeolite framework during the co-precipitation reaction.⁴⁰⁻⁴² The resonances at -111.2 and -117.7 ppm shift to higher field and increase in relative intensity after co-precipitation, we believe this is due to zeolite dealumination (Table S2). The Si/Al ratio of zeolite was calculated using the Loewenstein's rule (Eqn. S1). After surface growth of the Mg₂Al-CO₃ LDH shell, the Si/Al ratio of zeolite increased from 1.40 to 1.67, which is attributed to the dealumination of this Al-rich zeolite. An additional NMR resonance centred at 10 ppm is shown in the ²⁷Al DP-MAS NMR spectrum of Z13X@Mg₂Al-CO₃ LDH (Fig. S5). This is due to the addition of the octahedral-coordinated Al in the Mg₂Al-CO₃ LDH.

The thermal stability of Z13X@Mg₂Al-CO₃ LDH was studied using thermogravimetric analysis (TGA); three weight loss stages are observed (Fig. S6). Z13X@Mg₂Al-CO₃ LDH loses about 20 wt% when heated up to 200 °C (water); at around 370 °C, the dehydroxylation of Mg₂Al-CO₃ LDH completes and partial decarboxylation of Mg₂Al-CO₃ LDH takes place, this leads to a 12 wt% loss. The final stage gives 4 wt% loss which arises from the complete decarboxylation of Mg₂Al-CO₃ LDH.^{43,44} The TGA data suggests a 1:1 weight ratio between Z13X and Mg₂Al-CO₃ LDH. Based on the TGA,

ssNMR, inductively coupled plasma (ICP) analysis and elemental analysis results (Table S3), the chemical formula of Z13X, Z13X@Mg₂Al-CO₃ LDH and Mg₂Al-CO₃ LDH were determined (Table 1). We have determined that the core-shell product has less Na and Al than the parent Z13X, which is in agreement with the loss of Al and Na from the zeolite framework during co-precipitation as suggested by ²⁹Si solid-state NMR spectroscopy (Fig. 1).

The N₂ BET adsorption-desorption isotherm of Z13X@Mg₂Al-CO₃ LDH shows typical type I isotherm at relative pressure below 0.3 (Fig. S7), which is due to the micropore structure of Z13X. At relative pressures above 0.3, the core-shell composite exhibits a type IV isotherm with a H3 loop, due to the existence of slit mesopores in Mg₂Al-CO₃ LDH. A pore-size distribution can be from the Horvath Kawazoe modification, which is in agreement with the existence of micropores and mesopores in Z13X@Mg₂Al-CO₃ LDH (Fig. S8). Although an increase in Brauner-Emmett-Teller (BET) specific surface areas are observed for core@LDH hybrids containing non-porous cores (*e.g.* sphere silica,⁸ metal oxides^{45,46}), core@LDH hybrids with micro-/meso-porous core do not display the same porosity increase.^{7,11,47}

Z13X@Mg₂Al-CO₃ LDH possesses a lower specific surface area than Z13X itself (Table 2). In comparison a 1:1 wt physical mixture of Z13X and Mg₂Al-CO₃ LDH also showed a similar BET specific surface area as Z13X@Mg₂Al-CO₃ LDH. This suggest that the growth of the Mg₂Al-CO₃ LDH shell does not block access to the micropores within the zeolite. The external surface area of Z13X@Mg₂Al-CO₃ LDH is lower than physical mixture, Z13X and Mg₂Al LDH. This may be due to the loss of external zeolite surface area at the interface of LDH shell.⁴⁸

Effect metal nitrate addition rate and reaction ageing time

We have parameterised metal nitrate addition rate as the time taken to add the nitrate solutions (dropping time (D), ageing time is defined as (A). Per example a sample with a dropping time of 30 minutes and an ageing time of 16 h is called D0.5A16. The effect of dropping time was investigated using dropping times; 0.5, 1, 1.5 and 2 hours.

The XRD patterns of samples D2A1, D1.5A1, D1A1 and D0.5A1 are very similar (Fig. S9). Sections of these XRD pattern have been extracted (Fig. 2a) and show that a 0.5 h dropping time is enough to afford LDH with reasonable crystallinity. The morphology of the core-shell is shown in Fig. S11.

Table 1. Chemical formula of Z13X, Z13X@Mg₂Al-CO₃ LDH and Mg₂Al-CO₃ LDH

Sample name	Formula calculated
Z13X	H _{0.06} Na _{0.36} (AlO ₂) _{0.43} (SiO ₂) _{0.60} •1.0H ₂ O
Z13X@Mg ₂ Al-CO ₃ LDH	[H _{0.1} Na _{0.26} (AlO ₂) _{0.36} (SiO ₂) _{0.60}][Mg _{0.64} Al _{0.35} (OH) _{1.98} (CO ₃) _{0.18}]•1.5H ₂ O
Mg ₂ Al-CO ₃ LDH	Mg _{0.65} Al _{0.35} (OH) ₂ (CO ₃) _{0.18} •0.9H ₂ O

Table 2. Summary of the BET specific surface areas and pore volumes of Z13X, Z13X@Mg₂Al-CO₃ LDH and Mg₂Al-CO₃ LDH

Samples	Surface area (m ² g ⁻¹)				Micropore volume (cm ³ g ⁻¹)
	BET	External	Micropore		
Z13X	813	89	724		0.27
Z13X@Mg ₂ Al-CO ₃ LDH	458	72	386		0.15
Z13X/Mg ₂ Al-CO ₃ LDH physical mixture	456	84	372		0.15
Mg ₂ Al-CO ₃ LDH	125	109	16		0.01

The core-shell structure was readily achieved with a dropping time of only 0.5 h. Varying the dropping time does not affect the morphology of core-shells obtained.

An ageing time study was then conducted using a dropping time of 0.5 h, four ageing time were chosen (0.5, 1, 4 and 16 hours). The XRD pattern of samples with different ageing times are shown in Fig. S10. The Bragg diffraction peaks from the LDH show the same relative intensity for each of the samples D0.5A16, D0.5A4, D0.5A1 and D0.5A0.5 (Fig. 2b), indicating that 30 minutes is enough for LDH formation. The morphology of core-shells from different ageing times showed a similar thickness of LDH shell, and amount of free LDHs and LDH coverage on Z13X (Fig. S11). TGA results indicate that these seven core-shells exhibits the same composition and thermal stability (Fig. S12 and S13).

The BET specific surface area mainly derives from the micropore surface area (Table S3). Meanwhile, the micropore volume of core-shell show the same variation as the micropore surface area (Fig. 3). Amongst the samples prepared a different dropping times (Fig. 3a), D1A1 core-shell exhibits the highest surface area (505 m²/g). Further increasing the dropping time, both micropore and external surface area decrease. The external surface area mainly derives from Mg₂Al-CO₃ LDH shell and micropore surface area is mainly obtained from Z13X core.^{11,49} Regarding the external surface area, longer dropping times tends to give more aggregated LDHs with reduced BET surface area.^{9,50,51} We propose that the aggregation between LDH platelets block the micropores at the core-shell interface which causes a reduction in accessible micropore surface area.⁴⁸ Among samples with different ageing times (Fig. 3b), D0.5A0.5 exhibits the highest BET specific surface area (517 m²/g). Extending the ageing time from one to four

hours, results in a decrease in specific surface area from 494 to 466 m²/g respectively.

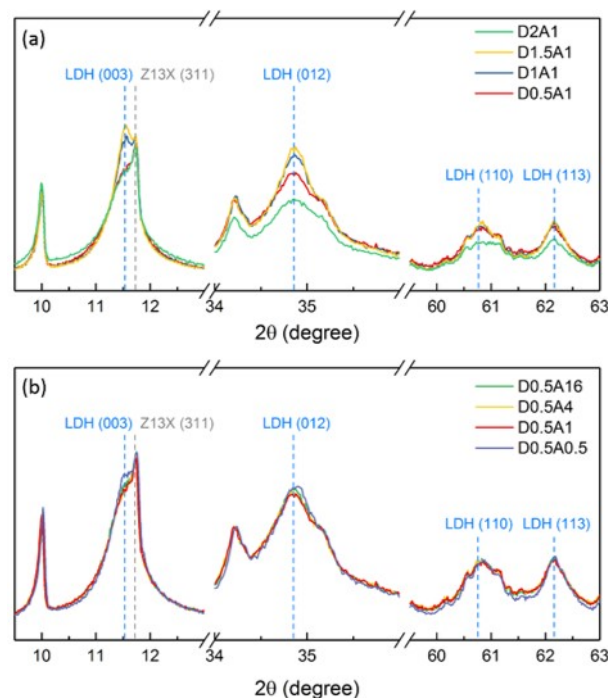
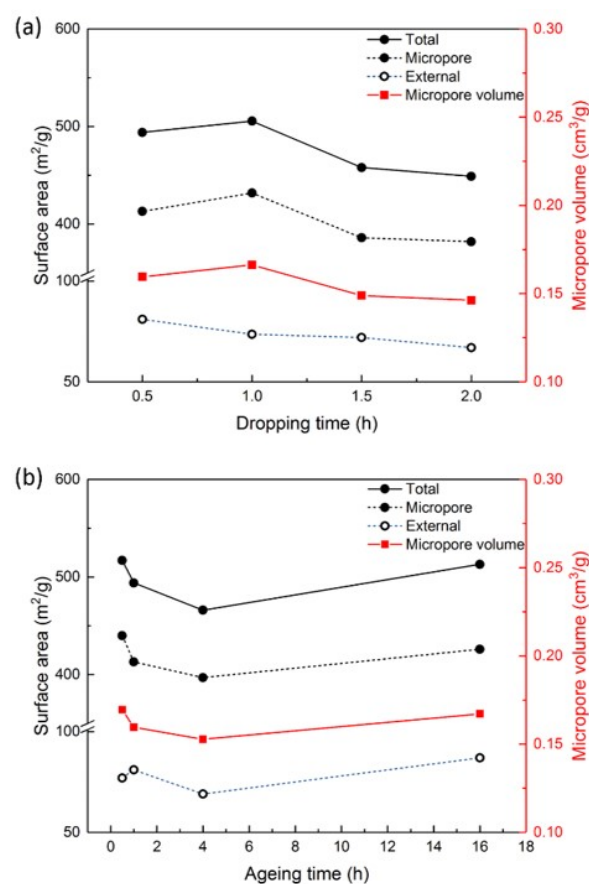
**Fig. 2.** Sections of the powder XRD pattern of (a) D2A1, D1.5A1, D1A1 and D0.5A1 sample and (b) D0.5A16, D0.5A4, D0.5A1 and D0.5A0.5 sample.

Fig. 3. Total BET specific surface area, micropore surface area, external surface area and micropore volume of (a) samples with varied dropping time, (b) samples with varied ageing time.

However, the BET specific surface area of D0.5A16 increases to 513 m²/g, perhaps due to Ostwald ripening type effects.¹² In highly alkaline Mg²⁺ and Al³⁺ nitrate solution, surface Si and Al sites on the zeolite became metastable and result in a partial dealumination as shown by ssNMR spectroscopy result. These metastable Al sites could act as the LDH nucleation sites. LDH nanosheets at the interface are small which are not able to block the zeolite micropores after 0.5 h ageing time. When the ageing time increases to 1 - 4 hours, LDH nanosheets undergo Ostwald ripening to form larger particles which start to block the micropores entrances. Ageing of 16 hours, a longer period of Ostwald ripening means the nanosheets grows bigger at the expense of small LDH nanosheets. Therefore, some of the blocked micropores can be released which results in an overall increase in BET specific surface area.

Synthesis of MOF@Mg₂Al-CO₃ LDH

Mg-MOF-74 was prepared using a solvothermal method previously reported by Yang and co-workers.³⁴ Rietveld refinement of the XRD confirms the synthesis of a single crystalline phase, Mg-MOF 74 (Fig. S14, Table S4). The obtained MOF are broccoli-like crystals with 40 – 50 µm particle size (Fig. 4a).

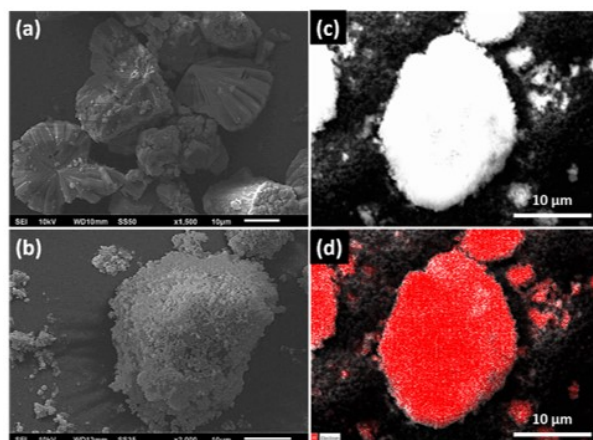


Fig. 4. (a) SEM image of Mg-MOF-74, (b) SEM images of Mg-MOF-74@Mg₂Al-CO₃ LDH, (c) SEM-EDS images of Mg-MOF-74@Mg₂Al-CO₃ LDH and (d) SEM-EDS Al mapping of MOF@Mg₂Al-CO₃ LDH.

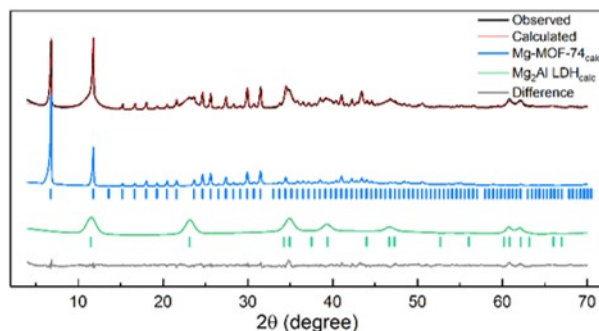


Fig. 5. XRD pattern and two-phase Reitveld refinement of MOF@Mg₂Al-CO₃ LDH. The observed, calculated and difference plots are shown in black, red and grey respectively. The calculated Mg-MOF-74 and Mg₂Al-CO₃ LDH single phase are shown in blue and green.

The XRD pattern of Mg-MOF-74@Mg₂Al-CO₃ LDH consists of the characteristic Bragg reflections of Mg-MOF-74 and Mg₂Al LDH, two-phase Reitveld refinement can be performed based on a weighted summation based of the scattering of Mg-MOF 74 and Mg₂Al-CO₃ LDH (Fig 5, Table S5). After co-precipitation, the surface became coarse and EDX mapping confirms the presence of the LDH on the surface (Fig 4b-c). Core-shell Mg-MOF-74@Mg₂Al-CO₃ LDH exhibits characteristic IR absorbance bands of Mg-MOF-74 and Mg₂Al LDH as shown in Fig. S15. TGA of Mg-MOF-74@Mg₂Al-CO₃ LDH indicated that this core-shell possesses three characteristic weight loss events (Fig. S16). The first one occurs between 100-200 °C (evaporation of solvent molecules), the second that takes place at around 350 °C, due to the continuous desorption of chemisorbed water within Mg-MOF-74, and the dehydroxylation and decarboxylation of Mg₂Al-CO₃ LDH. The final weight loss is due to the decomposition of the Mg-MOF-74 framework at 600 °C. The TGA data suggests a 1:1 wt ratio between Mg-MOF-74 and Mg₂Al-CO₃ LDH.

Conclusions

Z13X@Mg₂Al-CO₃ LDH was successfully obtained by a one-step, scalable co-precipitation method. The core-shell structure consists of a 250 nm-thick Mg₂Al-CO₃ LDH shell on a 2-4 µm octahedral Z13X core.

We observed a reduced BET specific surface area of the core-shell compared to pristine Z13X due to partial micropore blocking by the LDH nanosheets.

Z13X@Mg₂Al-CO₃ LDHs samples prepared using different Mg and Al nitrate addition rates and ageing time exhibit similar crystallinity, thermal stability and bulk composition. The highest BET specific surface area was observed for samples obtained by rapid Mg and Al nitrate addition followed by 16 hours ageing at pH 10. The high surface area of Z13X@Mg₂Al-CO₃ LDH can be readily prepared using rapid Mg and Al nitrate addition and 0.5 hour ageing. This synthetic method is also applicable to other porous core materials such Mg-MOF-74 to form Mg-MOF-74@Mg₂Al-CO₃ LDH.

Studies are ongoing to explore application of core@LDH materials as catalysts and gas sorption materials.

Experimental

Synthesis procedure of zeolite 13X@Mg₂Al-CO₃ LDH

Core-shell zeolite 13X@Mg₂Al-CO₃ LDHs were prepared using a modification of our previously published method.¹¹ Zeolite 13X (0.50 g) was dispersed in de-ionised (DI) water (100 mL) by sonicating the dispersion for 30 minutes. Na₂CO₃ (0.53 g, 5.00 mmol) was then added to the dispersion which

was sonicated for five minutes. This mixture (solution A) was adjusted to pH = 10 with 10 wt% nitric acid. An aqueous solution (96 mL) of $\text{Mg}(\text{NO}_3)_2 \cdot 6\text{H}_2\text{O}$ (1.23 g, 4.80 mmol) and $\text{Al}(\text{NO}_3)_3 \cdot 9\text{H}_2\text{O}$ (0.90 g, 2.40 mmol) was added to solution A within one and half hours (dropping rate of 64 mL/h). The pH value of the reaction mixture was kept constant at 10 by addition of 1 M NaOH(aq). After addition resulting mixture was allowed to age for one hour with gentle stirring. The product was collected by Buchner filtration and washed with water before being dried under vacuum at 30 °C overnight. The product was obtained as a white powder of $\text{Z13X@Mg}_2\text{Al-CO}_3$ LDH.

Synthesis of $\text{Z13X@Mg}_2\text{Al-CO}_3$ LDH with different reagent addition rates and ageing times

Effect of reagent addition rates: three different times for the Mg and Al nitrate addition (0.5, 1 and 2 hours) were investigated. The overall procedure is the same as $\text{Z13X@Mg}_2\text{Al-CO}_3$ -LDH mentioned above.

Effect of ageing time: three different ageing times (0.5, 4 and 24 hours) were investigated. The procedure is the same as $\text{Z13X@Mg}_2\text{Al-CO}_3$ -LDH mentioned above except using 0.5 hour dropping time and various ageing times.

Synthesis of $\text{Mg-MOF-74@Mg}_2\text{Al-CO}_3$ LDH

Mg-MOF 74 (0.10 g) was dispersed in DI water (20 mL) with thirty-minute sonication. Na_2CO_3 (0.10 g, 1.00 mmol) was then added to the dispersion and sonicated for another five minutes to form solution A. An aqueous solution (19.8 mL) of $\text{Mg}(\text{NO}_3)_2 \cdot 6\text{H}_2\text{O}$ (0.246 g, 0.96 mmol) and $\text{Al}(\text{NO}_3)_3 \cdot 9\text{H}_2\text{O}$ (0.18 g, 0.48 mmol) was added to solution A within thirty minutes (dropping rate 39.6 mL/h). The pH value of the reacting mixture was kept at 10 using 1 M NaOH(aq). The resulting mixture was stirred for half an hour after all the reagents were added. The product was collected by filtration and washed with water before being dried under vacuum at 30 °C overnight to form $\text{Mg-MOF-74@Mg}_2\text{Al-CO}_3$ LDH.

Conflicts of interest

The authors declare no competing financial interests.

Acknowledgements

M. L. acknowledges the Chinese Scholarship Council (CSC) for funding. C. C. and J.-C. B. would like to thank SCG Chemicals Co., Ltd. (Thailand) for funding. Dr Nicholas H. Rees (University of Oxford) is thanked for solid-state NMR spectroscopy analysis.

Notes and references

- 1 F. Cavani, F. Trifirò and A. Vaccari, *Catal. Today*, 1991, **11**, 173–301.
- 2 A. Garcia-Gallastegui, D. Iruretagoyena, M. Mokhtar, A. M. Asiri, S. N. Basahel, S. A. Al-Thabaiti, A. O. Alyoubi, D. Chadwick and M. S. P. Shaffer, *J. Mater. Chem.*, 2012, **22**, 13932–13940.
- 3 Y. Zhao, B. Li, Q. Wang, W. Gao, C. J. Wang, M. Wei, D. G. Evans, X. Duan and D. O'Hare, *Chem. Sci.*, 2014, **5**, 951–958.
- 4 Y. Wei, X. Zhang, X. Wu, D. Tang, K. Cai and Q. Zhang, *RSC Adv.*, 2016, **6**, 39317–39322.
- 5 Q. Wang, Y. Gao, J. Luo, Z. Zhong, A. Borgna, Z. Guo and D. O'Hare, *RSC Adv.*, 2013, **3**, 3414–3420.
- 6 X. Bi, H. Zhang and L. Dou, *Pharmaceutics*, 2014, **6**, 298–332.
- 7 H. Suo, H. Duan, C. Chen, J.-C. Buffet and D. O'Hare, *RSC Adv.*, 2019, **9**, 3749–3754.
- 8 C. Chen, R. Felton, J.-C. Buffet and D. O'Hare, *Chem. Commun.*, 2015, **51**, 3462–3465.
- 9 W. L. J. Kwok, D.-G. Crivoi, C. Chen, J.-C. Buffet and D. O'Hare, *Dalton. Trans.*, 2018, **47**, 143–149.
- 10 H. Suo, C. Chen, J.-C. Buffet and D. O'Hare, *Dalton. Trans.*, 2018, **47**, 16413–16417.
- 11 C. Chen, C. F. H. Byles, J.-C. Buffet, N. H. Rees, Y. Wu and D. O'Hare, *Chem. Sci.*, 2016, **7**, 1457–1461.
- 12 X. Liu, C. Wang, Y. Dou, A. Zhou, T. Pan, J. Han and M. Wei, *J. Mater. Chem. A*, 2014, **2**, 1682–1685.
- 13 X. Ge, Y. He, T. Plachy, N. Kazantseva, P. Saha and Q. Cheng, *Nanomaterials*, 2019, **9**, 527–541.
- 14 J. Cao, L. Li, Y. Xi, J. Li, X. Pan, D. Chen and W. Han, *Sustain. Energy Fuels*, 2018, **2**, 1350–1355.
- 15 C. Chen, P. Gunawan and R. Xu, *J. Mater. Chem.*, 2011, **21**, 1218–1225.
- 16 C. Chen, L. K. Yee, H. Gong, Y. Zhang and R. Xu, *Nanoscale*, 2013, **5**, 4314–4320.
- 17 Z. Gu, J. J. Atherton and Z. P. Xu, *Chem. Commun.*, 2015, **51**, 3024–3036.
- 18 J.-C. Buffet, C. F. H. Byles, R. Felton, C. Chen and D. O'Hare, *Chem. Commun.*, 2016, **52**, 4076–4079.
- 19 C. Wang, B. Ma, S. Xu, D. Li, S. He, Y. Zhao, J. Han, M. Wei, D. G. Evans and X. Duan, *Nano Energy*, 2017, **32**, 463–469.
- 20 X. Li, Z. Yang, W. Qi, Y. Li, Y. Wu, S. Zhou, S. Huang, J. Wei, H. Li and P. Yao, *Appl. Surf. Sci.*, 2016, **363**, 381–388.
- 21 Y. Ni, L. Yao, Y. Wang, B. Liu, M. Cao and C. Hu, *Nanoscale*, 2017, **9**, 11596–11604.
- 22 M. R. Othman, N. M. Rasid and W. J. N. Fernando, *Chem. Eng. Sci.*, 2006, **61**, 1555–1560.
- 23 B. Jha and D. N. Singh, in *Fly Ash Zeolites: Innovations, Applications, and Directions*, Springer, 1 st., 2016, pp. 5–31.
- 24 D. H. Olson, *J. Phys. Chem.*, 1970, **74**, 2758–2764.
- 25 N. Herron, G. D. Stucky and C. A. Tolman, *J. Chem. Soc., Chem. Commun.*, 1986, 1521–1522.
- 26 J. Haber, K. Pamin and J. Połtowicz, *J. Mol. Catal. A Chem.*, 2004, **224**, 153–159.
- 27 J. Merel, M. Clausse and F. Meunier, *Ind. Eng. Chem. Res.*, 2008, **47**, 209–215.
- 28 R. Ben-Mansour, M. A. Habib, O. E. Bamidele, M. Basha, N. A. A. Qasem, A. Peedikakkal, T. Laoui and M. Ali, *Appl. Energy*, 2016, **161**, 225–255.
- 29 Z. Bao, L. Yu, Q. Ren, X. Lu and S. Deng, *J. Colloid Interface Sci.*, 2011, **353**, 549–556.
- 30 U. Böhme, B. Barth, C. Paula, A. Kuhnt, W. Schwieger, A. Mundstock, J. Caro and M. Hartmann, *Langmuir*, 2013, **29**, 8592–8600.
- 31 D. Ruano, M. Díaz-García, A. Alfayate and M. Sánchez-Sánchez, *ChemCatChem*, 2015, **7**, 674–681.
- 32 C. Qu, B. Zhao, Y. Jiao, D. Chen, S. Dai, B. M. Deglee, Y. Chen, K. S. Walton, R. Zou and M. Liu, *ACS Energy Lett.*, 2017, **2**, 1263–1269.

- 33 M. C. Bernini, D. Fairen-Jimenez, M. Pasinetti, A. J. Ramirez-Pastor and R. Q. Snurr, *J. Mater. Chem. B*, 2014, **2**, 766–774.
- 34 D. A. Yang, H. Y. Cho, J. Kim, S. T. Yang and W. S. Ahn, *Energy Environ. Sci.*, 2012, **5**, 6465–6473.
- 35 G. S. Pawley, *J. Appl. Crystallogr.*, 1981, **14**, 357–361.
- 36 M. Safak Boroglu and M. Ali Gurkaynak, *Polym. Bull.*, 2011, **66**, 463–478.
- 37 S. Greiser, M. Hunger and C. Jäger, *Solid State Nucl. Magn. Reson.*, 2016, **79**, 6–10.
- 38 P. Pena, J. M. Rivas Mercury, A. H. de Aza, X. Turrillas, I. Sobrados and J. Sanz, *J. Solid State Chem.*, 2008, **181**, 1744–1752.
- 39 J. Huang, Y. Jiang, V. R. Reddy Marthala, Y. S. Ooi, J. Weitkamp and M. Hunger, *Microporous Mesoporous Mater.*, 2007, **104**, 129–136.
- 40 S. Lee, H. Kim and M. Choi, *J. Mater. Chem. A*, 2013, **1**, 12096–12102.
- 41 J. Klinowski, *Chem. Rev.*, 1991, **91**, 1459–1479.
- 42 C. A. Fyfe, Y. Feng, H. Grondy, G. T. Kokotailo and H. Gies, *Chem. Rev.*, 1991, **91**, 1525–1543.
- 43 C. Chen, M. Yang, Q. Wang, J.-C. Buffet and D. O'Hare, *J. Mater. Chem. A*, 2014, **2**, 15102–15110.
- 44 W. Yang, Y. Kim, P. K. T. Liu, M. Sahimi and T. T. Tsotsis, *Chem. Eng. Sci.*, 2002, **57**, 2945–2953.
- 45 Q. Yan, Z. Zhang, Y. Zhang, A. Umar, Z. Guo, D. O'Hare and Q. Wang, *Eur. J. Inorg. Chem.*, 2015, 4182–4191.
- 46 Q. Guo, Q. Zhang, H. Wang, Z. Liu and Z. Zhao, *Catal. Commun.*, 2016, **77**, 118–122.
- 47 R. Li, T. Xue, R. Bingre, Y. Gao, B. Louis and Q. Wang, *ACS Appl. Mater. Interfaces*, 2018, **10**, 34834–34839.
- 48 D. K. Panchariya, R. K. Rai, E. Anil Kumar and S. K. Singh, *ACS Omega*, 2018, **3**, 167–175.
- 49 Y. Zhai, S. Zhang, Y. Shang, Y. Song, W. Wang, T. Ma, L. Zhang, Y. Gong, J. Xu and F. Deng, *Catal. Sci. Technol.*, 2019, **9**, 659–671.
- 50 C. Chen, P. Wang, T.-T. Lim, L. Liu, S. Liu and R. Xu, *J. Mater. Chem. A*, 2013, **1**, 3877–3880.
- 51 C. Chen, A. Wangriya, J.-C. Buffet and D. O'Hare, *Dalton. Trans.*, 2015, **44**, 16392–16398.